EUROPEAN FUSION DEVELOPMENT AGREEMENT

EFDA–JET–PR(03)32

A. Loarte, G. Saibene, R. Sartori, D. Campbell, M. Becoulet, L. Horton, T. Eich, A. Herrmann, G.Matthews, N. Asakura, A. Chankin, A. Leonard, G. Porter, G. Federici, G. Janeschitz, M. Shimada and M. Sugihara

Characteristics of Type I ELM Energy and Particle Losses in Existing Devices and their Extrapolation to ITER

Characteristics of Type I ELM Energy & Particle Losses in Existing Devices and their Extrapolation to ITER

A. Loarte[1], G. Saibene[1], R. Sartori[1], D. Campbell[1], M. Becoulet[2], L. Horton[3], T. Eich[3], A. Herrmann[3], G.Matthews[4], N. Asakura[5], A. Chankin[5], A. Leonard[6], G. Porter[6-7], G. Federici[8], G. Janeschitz[9], M. Shimada[8] and M. Sugihara[8]

[1]*EFDA-CSU, Max-Planck-Institut für Plasmaphysik, D-85748 Garching, Germany*
[2]*Association Euratom-CEA, DRFC, CEA Cadarache, F-13108 St Paul lez Durance, France*
[3]*Max-Planck-Institut für Plasmaphysik, Euratom Assoziation, D-85748 Garching, Germany*
[4]*EURATOM/UKAEA Fusion Association, Culham, Abingdon, Oxon.OX14 3DB, UK*
[5]*Japan Atomic Energy Research Institute, Naka-machi, Naka-gun, Ibaraki-ken, 311-01, Japan*
[6]*General Atomics, P.O. Box 85608,San Diego, CA 92186-5608, USA*
[7]*Lawrence Livermore National Laboratory, P.O. Box 808,Livermore, CA 94551-9900, USA*
[8]*ITER-IT, Garching & Naka Working Sites, JEARI and MPI für Plasmaphysik, Germany & Japan*
[9]*Forschungszentrum Karlsruhe, P. O. Box 3640, 76021 Karlsruhe, Germany*

Preprint of Paper to be submitted for publication in
Plasma Physics and Controlled Fusion

ABSTRACT.

Analysis of Type I ELMs from present experiments shows that ELM energy losses are correlated with the density and temperature of the pedestal plasma before the ELM crash. The Type I ELM plasma energy loss normalised to the pedestal energy is found to correlate across experiments with the collisionality of the pedestal plasma (ν^*_{ped}), decreasing with increasing ν^*_{ped}. Other parameters affect the ELM size such as the edge magnetic shear, etc., that influence the plasma volume affected by the ELMs. ELM particle losses are influenced by this ELM affected volume and are weakly dependent on other pedestal plasma parameters. In some conditions in JET and DIII-D, ELMs can be observed ("Minimum" Type I ELMs with energy losses acceptable for ITER), in which ELMs do not affect the plasma temperature. The duration of the divertor ELM power pulse is correlated with the typical ion transport time from the pedestal to the divertor target ($\tau_{\|}^{Front} = {2\pi R q_{95}}/{c_{s,ped}}$) and not with the duration of the ELM-associated MHD activity. Similarly, the time scale of ELM particle fluxes is also determined by $\tau_{\|}^{Front}$. The extrapolation of present experimental results to ITER is summarised.

1. INTRODUCTION.

The Type I ELMy H-mode regime is the reference regime for inductive operation of some next step devices such as ITER [16]. The Type I ELMy H-mode is a regime obtained in many divertor tokamaks and has acceptable energy confinement at the high densities required in next step devices and fusion reactors, particularly at higher plasma triangularities [46, 22, 39, 50]. Type I ELMy H-modes show experimental performances with respect to steady state helium exhaust [52, 3, 48, 11] and divertor power deposition [42, 21, 45] which could meet the necessary requirements when extrapolated to next step devices such as ITER [23].

A major drawback of the Type I ELMy H-mode is the periodic large power loads on plasma facing components associated with the Type I ELMs [53, 13, 5, 26]. Determining the size of the expected Type I ELM power loads in ITER is the object of active research and this paper summarises recent progress in this direction. Divertor tokamak experiments show that Type I ELMs cause fast losses of energy (~ several hundred microseconds) from the confined plasma that amount typically to few percent of the plasma energy (as determined by diamagnetic loop measurements) [53]. A large part of this energy is deposited on the divertor target over an area similar or somewhat larger than that of steady-state power flow [14]. The power loads associated with Type I ELMs are, generally, of no concern for the lifetime of the divertor targets in present experiments, but may lead to unacceptable divertor target lifetime reduction when extrapolated to next step devices [16, 27, 20, 33, 8]. This divertor lifetime limitation in ITER is associated with the target surface temperature exceeding the sublimation (for a carbon divertor target) or melting (for a tungsten divertor target) temperature that leads to a large target erosion at every ELM. More details on the expected Type I ELM erosion rates in ITER and their dependence on energy flux characteristics can be found in a companion paper in this ELM cluster [8]. ELM driven particle losses from the core plasma have, on the contrary,

a positive influence on the performance of ELMy H-modes. The particle confinement time in H-modes is significantly increased with respect to L-mode and the ELMs provide the required particle outflux to achieve stationary plasma content [53]. The influence of the ELM driven particle fluxes on impurities is even more dramatic and, in the absence of ELMs, H-mode discharges suffer from impurity accumulation [53].

Understanding of the physics mechanisms behind the ELM particle and energy losses from the main plasma, the associated energy fluxes on the divertor target and main chamber plasma facing components and their extrapolation to ITER requires dedicated experiments in existing divertor tokamaks and the comparison of the relevant measurements from these experiments. In this paper, we present the results from an initial comparison of experimental results from ASDEX Upgrade, DIII-D, JET and JT-60U carried out within the International Tokamak Physics Activities (ITPA). The plasma parameters considered in this study are the core plasma ELM energy and particle losses (ΔW_{ELM} and ΔN_{ELM}) and the divertor ELM energy flux and its spatial and temporal characteristics. Measurements of Type I ELM characteristics are difficult and, hence, for some parameters, systematic studies are only available in one experimental device. In those cases, we summarise the findings in the relevant device and highlight the experiments/measurements needed in other experiments in order to provide a firm extrapolation from these results to ITER. The research in this area is on-going and the development of a physics model for the ELM energy and particle losses is far from complete. Hence, this paper represents the present understanding of the processes involved in the loss of energy from the main plasma based on observations in several divertor tokamaks. As more detailed experiments are carried out and better measurements are available, some areas of this understanding are bound to change.

2. CHARACTERISTICS AND INTRINSIC VARIABILITY OF TYPE I MAIN PLASMA ELM ENERGY LOSSES AND DIVERTOR ENERGY FLUXES.

The ELMs considered in this study are from discharges with dominant NBI heating in stationary plasma conditions. Under these conditions, experimental measurements show that ELM bulk plasma energy and particle losses and other main plasma ELM characteristics are reproducible, although not identical, as expected for a phenomenon triggered by a MHD instability. Figure 1(a) & 1(b) show the measured probability distribution function for the ELM frequency and ELM energy loss for an extensive set of JET experiments (~ 200 points from 50 discharges for Fig.1(a) and ~ 100 ELMs from these discharges for Fig.1(b) [34]. The standard deviation of these distribution functions is 10% for the ELM frequency and 15% for the ELM energy loss. The need to consider measurements for reproducible Type I ELMs in stationary conditions in this study is twofold: First, varying plasma conditions both in the main and pedestal plasmas are known to affect the characteristics of ELMs. Our study is orientated towards providing an extrapolation from present results to those expected in stationary conditions for the ITER Q_{DT} =10 reference regime and, hence, stationary ELMs should be used. Second, due to the fast time scale (typically, a few hundred microseconds) required to

measure ELM characteristics, the time resolution of many diagnostics is insufficient to determine such characteristics. In order to circumvent this problem, measurements with insufficient time resolution for many similar ELMs are combined allowing the determination of the required characteristics for an "average ELM". More details on the application of this technique can be found in [19, 44]. Obviously, this method relies on most of the ELMs combined being similar with a moderate scatter (such as those in Fig.1(a) and Fig.1(b)) around the average value that is determined by this technique.

The determination of the ELM energy and particle fluxes on the divertor target and their variability is extremely complicated because it requires high time resolution measurements over the whole target area. Such measurements usually exist at one (or few) toroidal locations and global divertor energy flux is derived under the assumption of toroidal symmetry for the energy flux during ELMs. Existing measurements of the divertor ELM energy flux with Infra-red cameras and particle fluxes with Langmuir probes show that the divertor ELM energy flux is approximately toroidally symmetric [26, 14, 38], as shown in Fig.2 by the probability distribution function of this asymmetry obtained from experiments in DIII-D [26] for ~ 50 ELMs. At present, it is not known if there is any correlation between the toroidal symmetry of the divertor ELM energy fluxes and other global ELM characteristics, such as the size of ΔW_{ELM} or the pedestal plasma parameters, or if the scatter shown in Fig.2 is due to the "natural" ELM variability and/or to issues related to the relative calibration of the two IR-camera diagnostics used in this study. Assuming that the divertor ELM energy flux is toroidally symmetric for all conditions, it is possible to determine the global energy balance during ELMs, i.e., how much of the energy lost from the main plasma reaches the divertor target. Both in JET and ASDEX Upgrade, it is found that more than 50% of ΔW_{ELM} reaches the divertor target [15, 7]. Interaction of the plasma expelled during an ELM with the main chamber PFCs has been seen in DIII-D and JET [30, 9]. An example of the probability distribution function for the energy arriving at the divertor (ΔW_{ELM}^{div}) versus main plasma energy loss (ΔW_{ELM}) from ASDEX Upgrade experiments [13] is shown in Fig.3 for ~ 20 ELMy H-mode discharges. As in the case of toroidal symmetry described above, it is not know if the scatter in this figure is associated with the "natural" ELM variability or if there is a dependence on other ELM characteristics. The data in Fig.3 and similar observations in JET [15, 7] imply that a non-negligible amount of the main plasma ELM energy loss may reach Plasma Facing Components (PFCs) in the main chamber of the device and not the divertor target. While this can enhance the range for ITER operation with acceptable divertor lifetime, it may restrict severely the lifetime of main chamber PFCs. Contrary to the divertor target, PFCs is the main chamber are usually not toroidally symmetric and the interaction of ELMs with these elements is concentrated in relatively small areas [9].

A larger experimental database exist for the poloidal profiles of the power flux during ELMs. In ASDEX Upgrade and JET it is observed that there is no (or just a small) broadening of the power flux profile to the divertor during ELMs as compared to that between ELMs [15, 7]. An example of the probability distribution function for the relative (to in-between ELMs) broadening of the divertor

ELM power width profile from ASDEX Upgrade experiments is shown in Fig.4 [14] for ~ 60 ELMs. As in the case of toroidal symmetry described above, it is not know if the scatter in this figure is associated with the "natural" ELM variability or if there is a dependence on other ELM characteristics. In some cases, large power profile shape modifications during Type I ELMs are observed [32, 5]. These have been interpreted as caused by large shifts of the divertor strike point position and research to understand these observations and their relevance for the expected ITER Type I ELMs is ongoing.

A more systematic characterisation of the probability distribution function of the ELM characteristics described in this section is necessary in order to evaluate the effect of the ELM "variability" on the ITER divertor lifetime predictions. While these studies are being carried out at the existing experimental devices, and in the absence of experimental evidence in conflict with them, the probability distribution functions shown in Figs.1–4 are taken as typical in order to estimate the expected "variability" of the ELM parameters and ELM divertor energy fluxes in ITER and the influence of this variability on the ITER divertor target lifetime [8]. The rest of this paper will describe the experimental observations of the "average" ELM characteristics in present devices and their extrapolation to ITER.

3. TYPE I ELM ENERGY AND PARTICLE LOSSES FROM THE MAIN PLASMA IN ELMY H-MODES.

For fixed Type I ELMy H-mode discharge conditions (P_{INPUT}, I_p, B_T, plasma shape, etc.) with flat or weakly peaked density profiles ($<n_e>$ a n_{ped}), the ELM energy losses (ΔW_{ELM}) are correlated with the average plasma density. Higher average (and pedestal) plasma densities correspond to smaller ELM energy losses in ASDEX Upgrade, DIII-D and JET [34, 28, 51], as shown in Fig.5(a) and 5(b) for JET and DIII-D experiments. In this plot the ELM energy loss, ΔW_{ELM}, is normalised to the pedestal energy W_{ped} ($W_{ped} = 3/2\ n_{e,ped}\ [T_{e,ped} + T_{i,ped}]\ V_{plasma}$) and not to the total plasma energy W_{dia}. This normalisation is more relevant for the study of ELMs losses, as ELMs are seen to cause a decrease in the plasma parameters only in the edge region. Normalising the ELM energy losses to W_{ped} has improved the understanding of inter-machine ELM observations by removing the scatter introduced when normalising the ELM energy losses to W_{dia}, due to varying degrees of profile stiffness among different experiments [27]. The decrease of ΔW_{ELM} with increasing plasma density is mostly due to the decrease of the ELM-associated temperature drop and not to the density drop both for JET and DIII-D as shown in Fig.5(a) and Fig.(b). This implies that not only the size of the ELM energy loss decreases with increasing density but also that the mechanism of the ELM energy loss depends on the density of the plasma in the pedestal region. As first identified in DIII-D [28] and confirmed in JET experiments [34], low/medium density Type I ELMs are mostly "conductive" ELMs (i.e., ΔW_{ELM} is associated with large $\Delta T_{e,ELM}$) while high density ELMs are mostly "convective" (i.e., ΔW_{ELM} is associated with small $\Delta T_{e,ELM}$). In both experiments there exist†"purely convective" Type I ELMs for high density experimental conditions. In these ELMs,

the plasma temperature remains unaffected by the ELMs, as shown in Figs. 6 and 7 both for "conductive" and "purely convective" ELMs in DIII-D and JET. For these ELMs, the measured ΔW_{ELM} is due to the loss of particles that the ELM causes (measured ΔN_{ELM}). These "purely convective" ELMs are the so-called "minimum" Type I ELMs [34] and, because of the weak dependence of the particle losses on pedestal plasma parameters discussed below, they determine the smallest possible main plasma energy loss that a Type I ELM can cause. Both for JET and DIII-D "minimum" Type I ELMs are associated with $\Delta W_{ELM}/W_{ped} = 0.04– 0.1$, which, if achievable in the ITER reference $Q_{DT} = 10$ scenario, would be compatible with an acceptable divertor target lifetime [17].

The reduction of the Type I ELM energy loss is not accompanied by a proportional reduction of the volume of plasma in which ELMs cause a sudden change of density and temperature, the so-called "ELM affected volume". ELMs affect the outermost ~ 10 – 30% of the plasma radius (20 - 45% of the total plasma volume) in DIII-D [29], JET [34] and JT-60U [4], as already shown in Figs.6 and 7. An example of the temperature profiles before an after an ELM in a JET fuelling scan and a low density discharge in JT-60U are shown in Fig.8(a) & Fig.8(b) shows the ELM temperature perturbation for the same experiments in a normalised form [36]. For discharges with similar pedestal plasma parameters, such as Pulse No: 53185 in JET and Pulse No: 37847 in JT-60U, the collapse of the plasma temperature at the edge region following an ELM is virtually identical in the two devices, both in size and shape, suggesting that the same physics mechanisms are behind the ELM observations in all experiments. The JET data in Fig.8(a) and Fig.8(b) correspond to a fuelling scan in Type I ELMy H-mode conditions. With increasing average (and pedestal) plasma density (increased fuelling rate) the absolute size of the temperature collapse decreases strongly (in a similar fashion to Fig.5(a)) but the shape of the perturbation to the temperature profile caused by the ELM, and with it the ELM affected volume, changes only weakly. This is shown in a more detailed way in Fig.9 for the normalised radius of the innermost surface affected by the ELM in a series of fuelling scans in a large range of conditions for JET [34]. As shown in this figure, the region affected by the ELMs depends on details of the magnetic configuration, plasma shape, etc., but changes only weakly with the level of gas fuelling. Similar qualitative trends have been observed in DIII-D [47, 31] but a quantitative multi-machine comparison of these observations remains to be carried out.

Experiments in divertor tokamaks show a decrease of the Type I ELM energy loss (normalised to W_{ped}) with increasing pedestal density. Fig.10 shows the normalised ELM energy loss versus pedestal density normalised to the Greenwald value for the discharges considered in this study. Although all experiments show a decrease of the ELM size with density, for similar pedestal densities (normalised to Greenwald) the measured ELM energy loss varies widely from experiment to experiment. An alternative parameter to compare inter-machine energy losses that has been proposed is the collisionality of the pedestal plasma ν^*_{ped} (neo) = $R\, q_{95}\, \varepsilon^{-3/2}\, (\lambda_{e,e})^{-1}$, where $\lambda_{e,e}$ is the electron-electron coulomb collision mean free path [33]. Figure 11 shows the same data as Fig.10 but plotted versus pedestal collisionality. The reduced differences among experiments seen in Fig.11

(with respect to Fig.10) indicate that the collisionality of the pedestal plasma seems to play a major role in determining the ELM energy loss across various experiments. Although no detailed physics model has been developed so far to explain this dependence, the pedestal plasma collisionality is expected to play a major role in ELM physics. Within the peeling-ballooning model of the ELM, the pedestal plasma collisionality is one of the parameters that determines the characteristics of the ELM trigger through its effect on the edge bootstrap current [6, 49, 40]. It has also been proposed that the pedestal plasma collisionality may play a major role in the transport of electron energy from the pedestal plasma to the divertor [24, 35] leading to smaller energy losses at higher plasma collisionalities.

Obviously, besides the plasma collisionality, other parameters such as the plasma shape, additional heating level, pedestal widths, etc., play a role in determining the ELM energy loss and are likely to be associated with the remaining scatter of the experimental measurements in Fig.11. Further experiments are in progress in all major devices to determine, in detail, the pedestal plasma parameters that influence the ELM energy loss and to control such loss, as far as possible. Injection of pellets is a well established technique to trigger ELMs and, possibly, to control the ELM energy loss, which could be used in ITER [43]. Experiments in ASDEX Upgrade and JET [25, 37] have indeed demonstrated such control of ELM frequency and ELM energy loss. Unfortunately, decreasing the ELM energy loss by frequent pellet injection leads to a deterioration of energy confinement and further optimisation of these experiments (if possible at all) is necessary before they can be considered as a viable scheme for ELM energy loss control in ITER.

Contrary to Type I ELM energy losses, particle losses seem to depend very weakly on pedestal plasma parameters. This is the reason for the relatively weak dependence of convective ELM energy losses on pedestal plasma parameters first identified in DIII-D [29]. Fig. 12 shows the ELM particle losses (ΔN_{ELM}) normalised to the pedestal particle content ($N_{ped} = n_{e,ped}\, V_{plasma}$) versus pedestal collisionality for a series of JET discharges illustrating this point. At present, there is no systematic inter-machine comparison of ELM particle losses, partly due to the difficulty of the measurement with the available diagnostics (interferometry and Thomson scattering) [44], although the qualitative behaviour seems similar in all experiments. It is important to understand the inter-machine scaling of the ELM particle losses, as this determines the value of the convective losses and, thus, the smallest possible Type I ELM energy loss [34].

4. TYPE I ELM POWER AND PARTICLE FLUXES ON PLASMA FACING COMPONENTS.

The study of ELM power and ELM particle fluxes onto first wall components is the topic of detailed studies [7, 15]. We only consider in this paper the outcome of the results from the inter-machine comparisons of the available measurements. Type I ELMs cause intense energy pulses on the divertor target with typical durations of several 100μs. The minimum timescale for the energy flux to the divertor is determined by that of the collapse of the pedestal plasma. The transport of energy from

the pedestal plasma to the divertor will only increase the duration of the phase with large divertor energy flux. The timescale for the collapse of the pedestal plasma can be determined by the decrease of the electron and ion temperatures and densities in the edge region and/or of other parameters linked to the values of pedestal temperature and density, such as the emissivity of soft X-rays. The duration of the collapse phase of the pedestal plasma parameters is typically 200–400μs in most experiments [34, 41, 28] and coincides with the duration of enhanced MHD activity and with that of the flux of energetic electrons onto the divertor target, as measured by the emission of bremsstrahlung soft X-rays [10, 34]. An example showing the collapse of the pedestal plasma for a JET discharge is shown in Fig.13 [35]. No systematic multi-machine comparison of the pedestal collapse time and of the duration of the enhanced MHD activity associated with the ELM has been carried out so far, but this time seems to be weakly dependent on pedestal parameters as shown in Fig.14 for the JET experiments [35].

Despite the independence of the pedestal collapse duration on pedestal plasma parameters, the time scale for the ELM energy flux to the divertor target is well correlated with pedestal plasma characteristics [7, 15, 34], as it will demonstrated below. In order to facilitate the inter-machine comparisons, the duration of the divertor ELM energy flux is characterised by the rise time of the divertor surface temperature, as measured with IR diagnostics (τ_{IR}^{ELM}). For a detailed analysis of the ELM power flux during ELMs in JET and ASDEX Upgrade the reader is referred to [7, 15]. Figure 15 shows an example of the divertor target surface temperature evolution and calculated ELM power flux for a JET Type I ELM [7] together with the illustration of the definition of τ_{IR}^{ELM} for this case. As shown in Fig.15, the temporal evolution of the power flux during Type I ELMs is much more complicated than what is reflected in a simple way in τ_{IR}^{ELM}. In particular, the power flux during an ELM is substantially different from a square waveform in time and a substantial amount of the ELM energy arrives to the divertor target after the maximum temperature has been reached [7]. This has sizeable and positive implications for the expected power fluxes during Type I ELMs and the subsequent damage expected at the divertor target in ITER [17]. Measurements of τ_{IR}^{ELM} over a large range of pedestal plasma parameters in ASDEX Upgrade, JET and JT-60U show that the duration of the ELM energy pulse on the divertor target is well correlated with the transit time for pedestal ions to reach the divertor target ($\tau_{\|}^{Front} = 2\pi R q_{95} / c_{s,ped}$) and not with the duration of the ELM MHD event and/or the duration of the flux of hot electrons on the divertor target [36]. Figure 16 shows the measured τ_{IR}^{ELM} versus the calculated $\tau_{\|}^{Front}$ for the available multi-machine dataset. For the calculation of $\tau_{\|}^{Front}$, the values of the pedestal electron and ion temperatures before the ELM are used ($T_{e,ped} = T_{i,ped}$ is assumed when no pedestal ion temperature measurements are available). The experimental scaling derived from these measurements is τ_{IR}^{ELM} (μs) = 0.29 [$\tau_{\|}^{Front}$ (μs)]$^{1.38}$. The correlation of the divertor ELM energy flux time (τ_{IR}^{ELM}) with $\tau_{\|}^{Front}$ reveals that the duration of the ELM power flux pulse is controlled by the parallel ion dynamics during the ELM event. Such finding is in agreement with kinetic simulations of the divertor power flux during ELMs carried out under the assumptions that a high energy sheath is established at the

divertor target during the ELM and that secondary electron emission remains moderately low during this phase [2]. Simultaneous measurements of the ion flux entering the divertor with Langmuir probes and of the divertor ELM power deposition with an IR camera in JT-60U are also in agreement with the hypothesis of the dynamics of the ion flow controlling the energy flux to the divertor during ELMs [1]. This set of observations indicates that the ionisation of neutrals in the divertor plasma and/or of those created by the desorption of neutrals trapped in the target by the high energy electron flux do not play a major role on the ELM energy flux duration, but further research is needed to confirm this hypothesis.

Indeed the dynamics of the ion flux to the divertor target during ELMs seems to be deeply influenced by the ion flow from the pedestal plasma to the divertor and not by local ionisation/ desorption of neutrals in the divertor. Measurements of the high energy electron flux, ion and divertor D_α emission at the inner and outer divertors show that the arrival of hot electrons to both divertors coincides with the rise of ion flux and D_α emission at both divertors only for low pedestal densities and high pedestal temperatures. As a consequence, for low pedestal densities and high pedestal temperatures, the ion and D_α emission rise is simultaneous at both divertors as shown in Fig.17(a) for a JET Type I ELM [34]. At higher pedestal densities and low pedestal temperatures a significant delay appears between the hot electron pulse to the **inner** divertor (simultaneous with the ion flux and D_α emission rise at the **outer** divertor) and the ion flux and D_α emission rise at the **inner** divertor. As a consequence, a significant delay appears between the ion flux and D_α rise between inner and outer divertors for low pedestal temperatures and high pedestal densities as shown in Fig.17(b) for JET [34]. This phenomenon originally found in JET [34] and JT-60U [4] has been identified in ASDEX Upgrade [18] and DIII-D [12] as well, as shown in Fig.18. The occurrence of this delay in the arrival of the ion flux to the inner divertor and its correlation with the ion transit time from the pedestal to the divertor target is consistent with the expulsion of ELM particles being concentrated at the outer region of the torus and reaching the inner (furthest from the point of expulsion) and outer divertor by flowing from this point along the field lines.

5. EXTRAPOLATION OF THE TYPE I ELM ENERGY LOSSES AND ENERGY FLUXES FROM PRESENT EXPERIMENTS TO ITER.

Although a consistent picture for the ELM energy and particle losses and the associated fluxes on plasma facing components from all divertor tokamaks is emerging, the extrapolation of present results to ITER remains uncertain. The experimental evidence for the duration of the ELM energy flux provides a reliable and physics based means of extrapolating present experimental results to ITER. For the expected pedestal parameters in ITER ($n_{ped} = 8\times10^{19}$ m^{-3}, $T_{ped} = 3.5$keV), the duration of the ELM power pulse in ITER is $\tau^{ELM}_{IR} = 506\mu$ms. This, together with more realistic assumptions on the ELM power pulse temporal shape, ELM energy loss to the main chamber walls, ELM power profile broadening [Eich 2003, Herrmann 2003] and the possibility of modifying the ITER divertor towards more glancing poloidal angles, have lead to a recent re-assessment of the estimates of the

allowed ELM energy loss for acceptable divertor lifetime in ITER, including the ELM variability described in Section 2 [8]. These estimates will be reviewed further, as more experimental data on the temporal and spatial distribution of the divertor ELM energy flux become available and the physics models are refined accordingly.

Extrapolation of the ELM energy loss from the main plasma based on present experiments to ITER remains quite uncertain. In the absence of a validated physics model for the ELM energy loss, the extrapolation to ITER is being carried out along two lines :

a) The first line uses the experimental correlation of ELM energy loss with the pedestal collisionality shown in Fig.11 and assumes that it is a valid empirical law to extrapolate present results to ITER. In ITER, ν^*_{ped} (neo) = 0.062 and, hence, the expected ΔW_{ELM} would be 22MJ (for W_{ped}^{ITER} = 112 MJ). The approach is justified on the basis that this empirical correlation is the result of complex effects of the pedestal collisionality on the nature of the MHD trigger of the ELM as well as, possibly, the transport of energy in the ergodised layer at the plasma edge that the strong MHD disturbance is likely to create [6, 24].

b) The second line is based on the observation of a varying timescale for the transport of ELM energy to the divertor with pedestal plasma parameters for an approximately constant pedestal collapse time (as discussed in Section 4) [20]. Under this hypothesis, the transport of energy through the divertor sheath limits the size of the ELM energy loss if its characteristics time is similar or longer than the time during which the pedestal plasma is connected to the divertor target (or ELM MHD duration). The normalised energy losses are reasonably well correlated with $\tau_{||}^{Front}$, as expected from this physics picture, although some experiments deviate clearly from this correlation, as shown in Fig.19. The reasons behind these deviations are being investigated. This new re-examination of the ELM energy losses by considering $\tau_{||}^{Front}$ to be the relevant time for ELM energy transport has clear implications for the extrapolation of present results to ITER. $\tau_{||}^{Front}$ in present experiments is usually shorter than the ITER value (due to the shorter connection length). If $\tau_{||}^{Front}$ is the relevant parameter on which to extrapolate present results to ITER, this would mean that the ELM energy losses in ITER would be in the range typical of high density conditions in existing experiments ($\Delta W_{ELM}/W_{ped}$ ~ 5–10%), i.e., ΔW_{ELM}^{ITER} = 5– 11 MJ.

It is now clearly established that the energy transport during ELMs affects, or is correlated with, the size of the ELM energy loss. As shown in Section 3, the energy loss for “convection dominated” ELMs is significantly smaller than that for “conduction dominated” ones. It is thus possible that the change of transport mechanisms correlated with the change in pedestal parameters before the ELM (by themselves or through their influence on the ELM MHD trigger) cause a limitation to the ELM energy loss itself. However, the sheath impedance to energy flux cannot be the only factor that limits the energy transport during ELMs. The transport of energy through the sheath is strongly linked to the transport of ions through it. If the sheath were the only limitation to the flux of energy from the pedestal to the divertor target during ELMs, then ELM energy and particle losses should

decrease in the same way with increasing $\tau_{\|}^{Front}$. As already mentioned in Section 3, and explicitly shown in Fig.20 for a series of JET experiments [35], the ELM particle losses are very weakly dependent on pedestal parameters and, hence, on $\tau_{\|}^{Front}$ in clear contrast with the ELM energy loss shown in Fig.19. Understanding the transport of energy from the pedestal plasma to the divertor during the ELM remains an open question. Until a validated physics model for these processes is available, it is not possible to quantify the role that the finite rate for the transport of energy from the pedestal plasma to the divertor may play in determining the ELM energy loss and, hence, its possible implications for the expected ELM energy loss in ITER.

CONCLUSIONS.

Measurements of the ELM energy losses in ASDEX Upgrade, DIII-D, JET and JT-60U have demonstrated that such losses are determined by the pedestal plasma parameters before the ELM. In particular, the pedestal plasma collisionality (ν^*_{ped}) seems to be a good ordering parameter for the ELM energy losses when comparing measurements across experimental devices. The decrease of ΔW_{ELM} with increasing ν^*_{ped} comes mostly from a reduction of the plasma temperature drop caused by the ELM, while the (normalised) ELM particle losses seem to be weakly dependent on pedestal plasma parameters. Type I ELMs for which ΔW_{ELM} comes entirely from the loss of particles (with no temperature change) have been observed ("Minimum" Type I ELMs) in DIII-D and JET.

The influence of the pedestal plasma parameters on the particle and power fluxes onto the divertor target has been confirmed experimentally. Measurements of the ELM power flux pulse on the divertor target have shown that the duration of this pulse is correlated with the transport of particles during the ELM event and not with the duration of the MHD activity and the loss of high energy electrons from the pedestal plasma, as previously thought. Two areas where major uncertainties remain, in the extrapolation from present measurements of ELM power fluxes to plasma facing components to ITER, are : a) The poloidal distribution of the ELM divertor energy flux (i.e., inner/outer divertor asymmetry) and b) The flux of energy to the main chamber plasma facing components during ELMs.

The extrapolation of present experimental results to ITER remains uncertain because of the lack of a validated physics model for the ELM collapse and the transport of energy from the pedestal plasma to the divertor target during the ELM itself. Two possible lines have been explored : one based on empirical correlations of the measured ELM energy loss with pedestal collisionality and the other with the ion transport transit time from the pedestal to the divertor. Present estimates with these two lines for ITER expand a wide range of values from acceptable for divertor lifetime considerations 5 –11MJ (if $\tau_{\|}^{Front}$ determines the ELM energy loss) to unacceptable (22 MJ, if ν^*_{ped} controls the ELM energy size). Further experimental measurements from existing devices and experiments must be carried out to discriminate whether the observed decrease of ELM energy loss with increasing plasma density or pedestal collisionality is due to changes in the MHD nature of the ELM event or to the change of energy transport from the pedestal plasma to the divertor related to the pedestal plasma parameters themselves.

REFERENCES.

[1]. Asakura, N., et al., Plasma Phys. Control. Fusion **44** (2002) A313.

[2]. Bergmann, A., Nucl. Fusion **42** (2002) 1162.

[3]. Bosch, H.-S., et al., Jour. Nucl. Mat. **266-269** (1999) 462.

[4]. Chankin, A., et al., Nucl. Fusion **42** (2002) 733.

[5]. Clement, S., et al., Jour. Nucl. Mat. **266-269** (1999) 285.

[6]. Connor, J.W., Plasma Phys. Control. Fusion **40** (1998) 191.

[7]. Eich, T., et al., Jour. Nucl. Mat. **313-316** (2003) 919.

[8]. Federici, G., et al., to be published in this cluster.

[9]. Ghendrih, Ph., et al., Jour. Nucl. Mat. **313-316** (2003) 914.

[10]. Gill, R., et al., Nucl. Fusion **38** (1998) 1461.

[11]. Groth, M., et al., Nucl. Fusion **42** (2002) 591.

[12]. Groth, M., et al., Jour. Nucl. Mat. **313-316** (2003) 1071.

[13]. Herrmann, A., et al., Proc. 24th EPS Conf. on Controlled Fusion and Plasma Physics, Berchtesgaden, Germany, 1997, Vol. IV, p. 1417.

[14]. Herrmann, A., Plasma Phys. Control. Fusion **44** (2002) 883.

[15]. Herrmann, A., et al., Jour. Nucl. Mat. **313-316** (2003) 759.

[16]. ITER Physics Basis1999., Nucl. Fusion **39** (1999) 2137.

[17]. Federici, G., et al., to be published in this cluster.

[18]. Horton, L.D., et al., Proc. 9th European Fusion Physics Workshop, Saariselka, Finland, 2001.

[19]. Jachmich, S., et al., Proc. 28th EPS Conf. on Controlled Fusion and Plasma Physics, Madeira, Portugal, 2001, P4.079.

[20]. Janeschitz, G., et al., Jour. Nucl. Mat. **290-293** (2001) 1.

[21]. Kallenbach, A., et al., Nucl. Fusion **39** (1999) 901.

[22]. Kamada, Y., et al., Plasma Phys. Control. Fusion **41** (1999) B77.

[23]. Kukushkin, A., et al., Jour. Nucl. Mat. **290-293** (2001) 887.

[24]. Lackner, K., private communication.

[25]. Lang, P., et al., submitted to Nucl. Fusion, 2003.

[26]. Leonard, A., et al., Jour. Nucl. Mat. **241-243** (1997) 628.

[27]. Leonard, A., et al., Jour. Nucl. Mat. **266-269** (1999) 109.

[28]. Leonard, A., et al., Jour. Nucl. Mat. **266-269** (2001) 1097.

[29]. Leonard, A., et al., Plasma Phys. Control. Fusion **44** (2002) 945.

[30]. Leonard, A., et al., to be published in Phys. Plasmas, 2003.

[31]. Leonard, A., et al., Jour. Nucl. Mat. **313-316** (2003) 768.

[32]. Lingertat, J., et al., Jour. Nucl. Mat. **241-243** (1997) 402.

[33]. Loarte, A., et al., Fusion Energy 2000, ITERP/11(R), Proc. 18th IAEA Fusion Energy Conference (Sorrento, Italy, 2000), IAEA, Vienna 2001 (ISSN 1562-4153).

[34]. Loarte, A., et al., Plasma Phys. Control. Fusion **44** (2002) 1815.

[35]. Loarte, A., et al., Fusion Energy 2002, Proc. 19th IAEA Fusion Energy Conference (Lyon, France, 2002), to be published.
[36]. Loarte, A., et al., Jour. Nucl. Mat. **313-316** (2003) 962.
[37]. Loarte, A., et al., to be published, 2003.
[38]. Monk, R., PhD Thesis, Royal Holloway College, University of London, 1996.
[39]. Osborne, T., et al., Plasma Phys. Control. Fusion **42** (2000) A175.
[40]. Osborne, T., et al., Fusion Energy 2002, Proc. 19th IAEA Fusion Energy Conference (Lyon, France, 2002), to be published.
[41]. Oyama, N., et al., Plasma Phys. Control. Fusion **43** (2001) 717.
[42]. Petrie, T., et al., Nucl. Fusion **37** (1997) 321.
[43]. Polevoi, A., et al., Fusion Energy 2002, Proc. 19th IAEA Fusion Energy Conference (Lyon, France, 2002).
[44]. Porter, G., et al., Phys. Plasmas **8** (2001) 5140.
[45]. Riccardo, V., et al., Plasma Phys. Control. Fusion **43** (2001) 881.
[46]. Saibene, G., et al., Nucl. Fusion **39** (1999) 1133.
[47]. Saibene, G., et al., 9th EU-US Transport Task Force Workshop, CÛrdoba, Spain 2002.
[48]. Sakasai, A., et al., Jour. Nucl. Mat. **266-269** (1999) 312.
[49]. Snyder, P. B., et al., Phys. Plasmas **9** (2002) 2037.
[50]. Stober, J., et al., Plasma Phys. Control. Fusion **42** (2000) A211.
[51]. Urano, H., et al., to be published in this cluster.
[52]. Wade, M., et al., Nucl. Fusion **38** (1998) 1839.
[53]. Zohm, H., Plasma Phys. Control. Fusion **38** (1996) 1213.

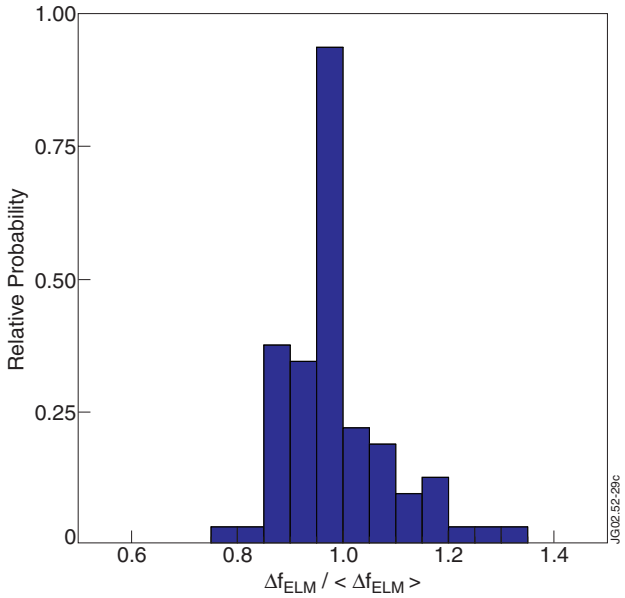

Figure 1: (a) Histogram of the probability distribution function of the ELM frequency for a series of stationary JET discharges. The typical standard deviation of the ELM frequency during the steady state phases of JET discharges is 10%.

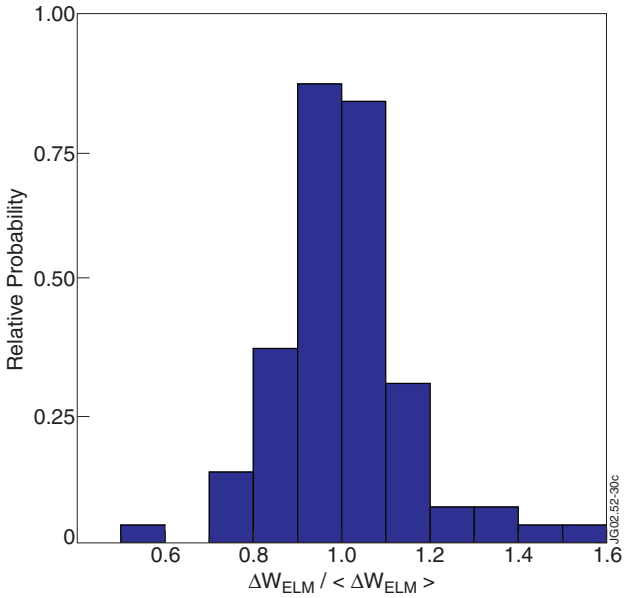

Figure 1: (b) Histogram of the probability distribution function of the ELM Energy loss for a series of stationary JET discharges. The typical standard deviation of the ELM Energy loss during the steady state phases of JET discharges is 15%.

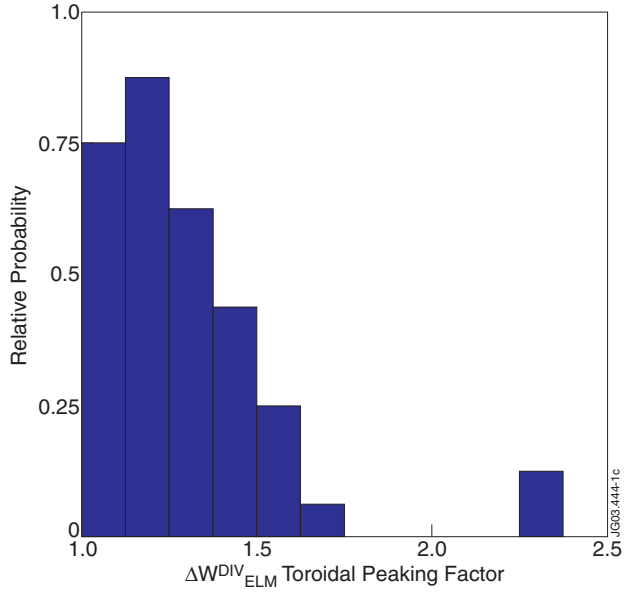

Figure 2: Histogram of the probability distribution function of the toroidal peaking factor (toroidal asymmetry from measurements at two toroidal locations) for ELM energy deposition at the divertor target in DIII-D discharges.

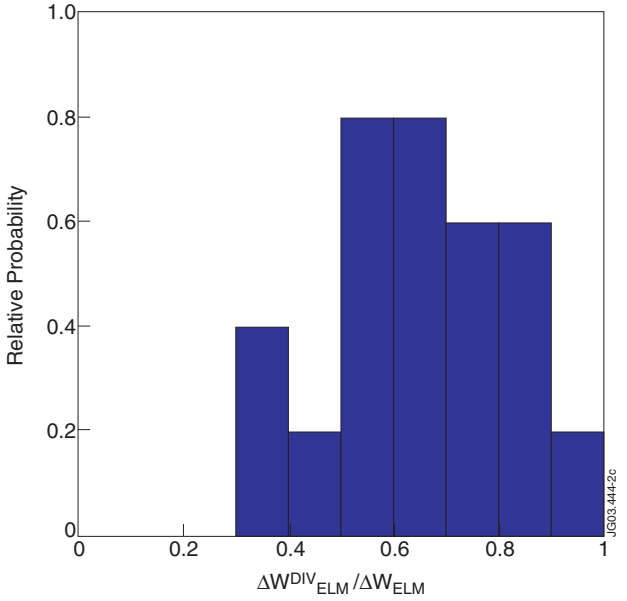

Figure 3: Histogram of the probability distribution function of the proportion of main plasma ELM energy loss (ΔW_{ELM}) that reaches the divertor target (ΔW^{DIV}_{ELM}) for ASDEX Upgrade discharges.

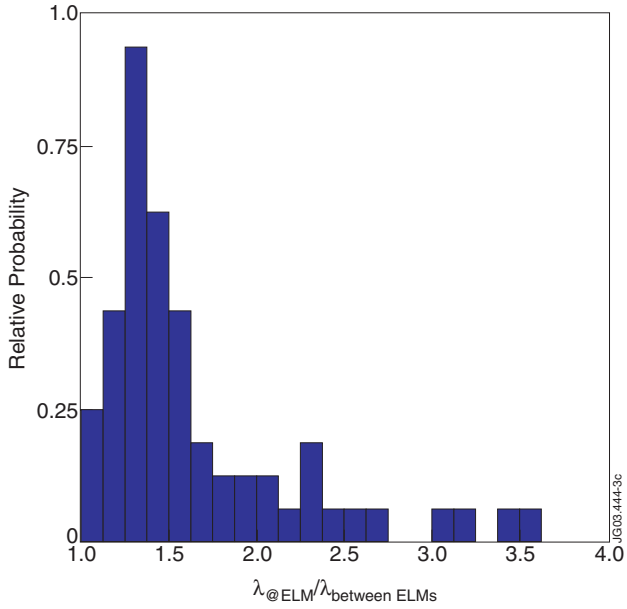

Figure 4: Histogram of the probability distribution function of the width for divertor energy flux during ELMs ($\lambda_{@ELM}$) compared to that in-between ELMs ($\lambda_{between\ ELMs}$) for ASDEX Upgrade discharges.

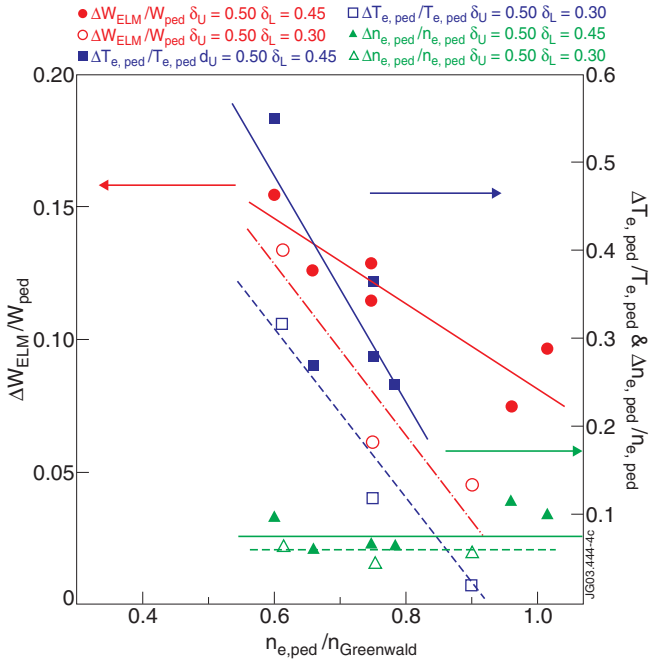

Figure 5: (a) Normalised ELM energy loss ($\Delta W_{ELM}/W_{ped}$) and pedestal temperature ($\Delta T_{e,ped}/T_{e,ped}$) and density ($\Delta n_{e,ped}/n_{e,ped}$) drop versus pedestal density normalised to the Greenwald limit ($n_{e,ped}/n_{Greenwald}$) for JET discharges with high upper and high/medium lower triangularities. The decrease of $\Delta W_{ELM}/W_{ped}$ with $n_{e,ped}$ is associated with the decrease of $\Delta T_{e,ped}/T_{e,ped}$, as $\Delta n_{e,ped}/n_{e,ped}$ seems independent of $n_{e,ped}$. At the highest $n_{e,ped}$, the ELM energy loss is due almost entirely to the ELM particle loss for discharges with medium lower triangularities. Lines are to guide the eye.

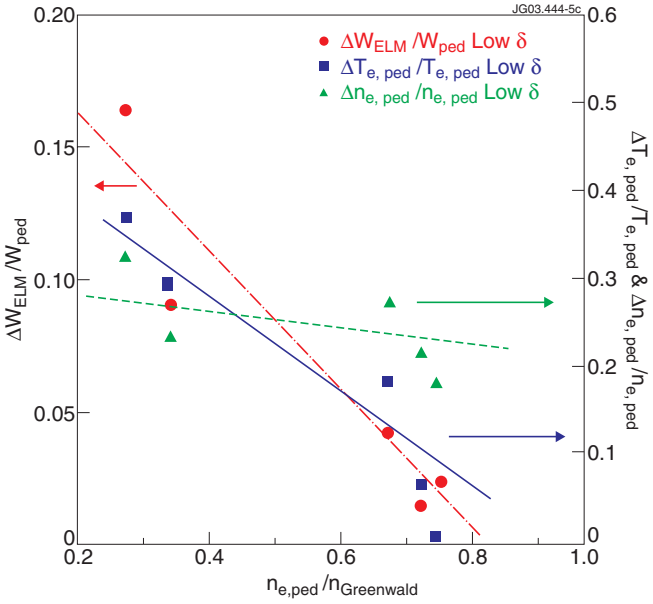

Figure 5: (b) Normalised ELM energy loss ($\Delta W_{ELM}/W_{ped}$) and pedestal temperature ($\Delta T_{e,ped}/T_{e,ped}$) and density ($\Delta n_{e,ped}/n_{e,ped}$) drop versus pedestal density normalised to the Greenwald limit ($n_{e,ped}/n_{Greenwald}$) for low triangularity DIII-D discharges. The decrease of $\Delta W_{ELM}/W_{ped}$ with $n_{e,ped}$ is associated with the decrease of $\Delta T_{e,ped}/T_{e,ped}$, as $\Delta n_{e,ped}/n_{e,ped}$ seems independent of $n_{e,ped}$. At the highest $n_{e,ped}$, the ELM energy loss is due almost entirely to the ELM particle loss. Lines are to guide the eye.

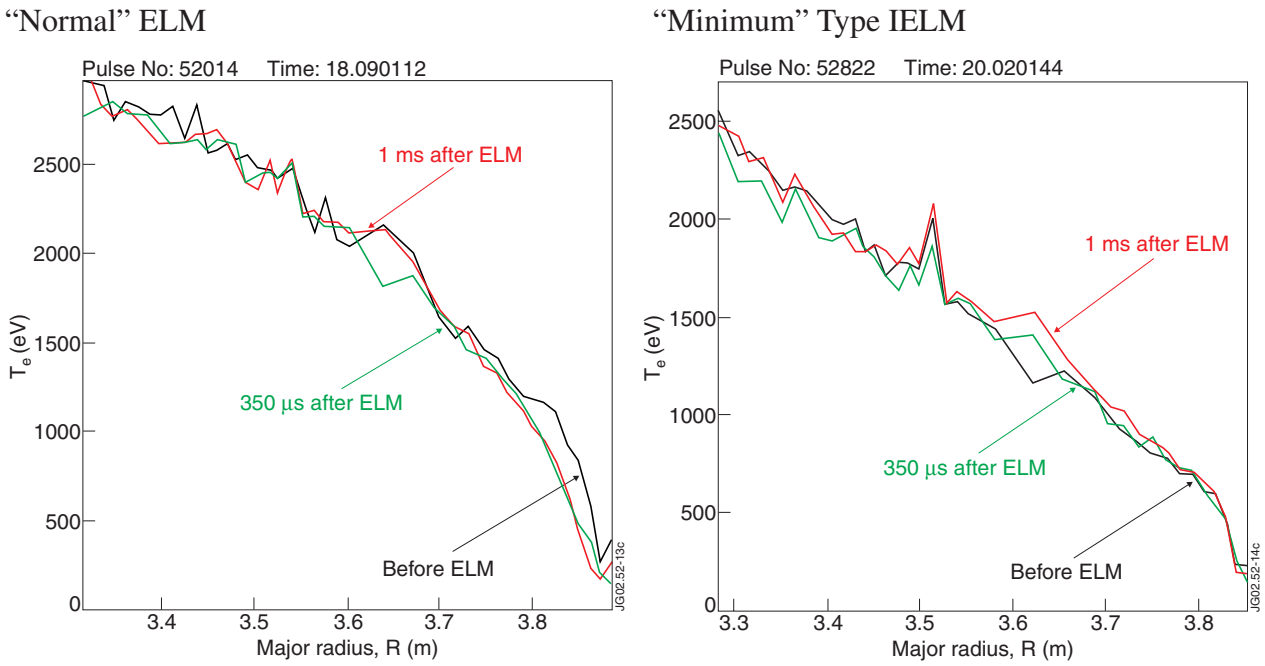

Figure 6. (Left) Electron temperature measurements in JET ELMy H-modes showing the collapse of the edge temperature in the outermost 15% of the plasma radius caused by a "Conductive" Type I ELM in a discharge with $\langle n_e \rangle = n_{Greenwald}$ and $\langle \delta \rangle = 0.47$. (Right) Electron temperature measurements in JET ELMy H-modes showing the absence of a collapse of the edge temperature in the outermost region of the plasma following at the occurrence of a† "Minimum" Type I ELM in a discharge with $\langle n_e \rangle = n_{Greenwald}$ and $\langle \delta \rangle = 0.40$ ($\delta_L = 0.30$). The magnetic axis is at R = 3.09 m for both discharges.

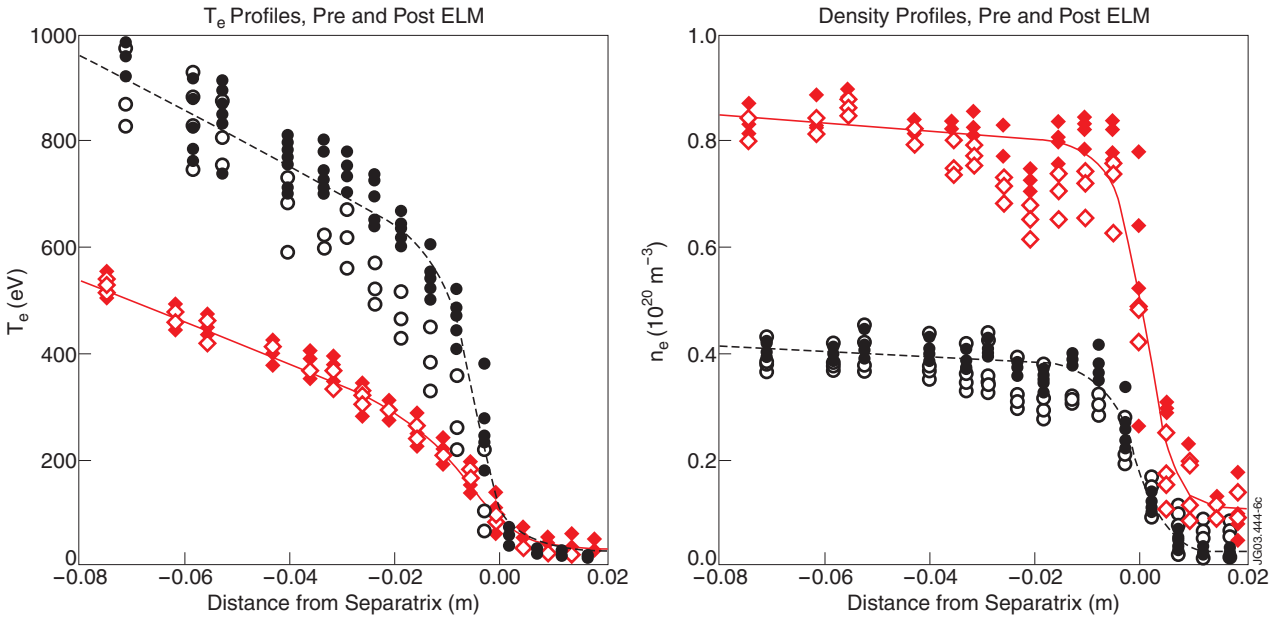

Figure 7. Edge electron temperature and density profile measurements in DIII-D Type I ELMy H-modes showing the collapse of the edge temperature and density caused by the ELMs. Full symbols correspond to measurements before the ELMs and open symbols correspond to measurements after the ELMs. Black symbols correspond to the ELM collapse of the edge profiles observed at low densities (i.e., "Conductive" ELMs), while red symbols correspond to high densities. At high densities (red symbols), no measurable change of the electron temperature is seen to occur at the ELM (i.e., "Minimum" Type I ELM) and the ELM energy loss is entirely due to the loss of particles, as shown by the decrease of edge density.

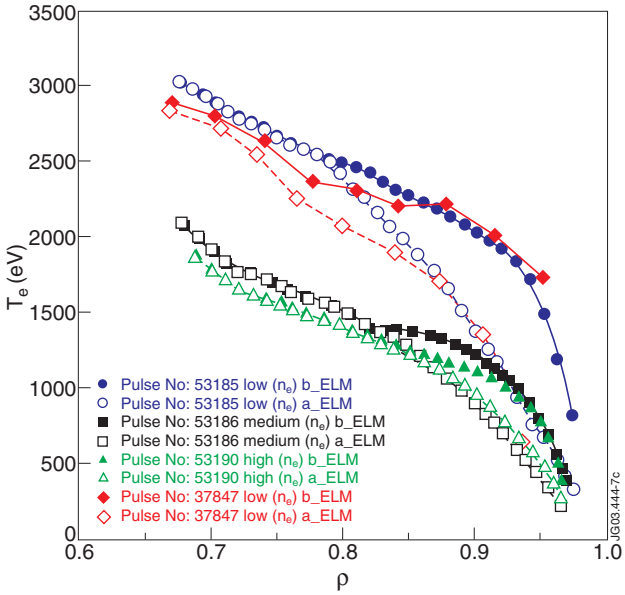

Figure 8: (a) Electron temperature measurements in JET and JT-60U ELMy H-modes versus normalised radius (ρ = r/a) showing the collapse of the edge temperature in the outermost 20% of the plasma radius caused by Type I ELMs. The JET measurements correspond to a density scan in Type I ELMy H-mode conditions, while the JT-60U correspond to a Type I ELMy H-mode discharge at low density.

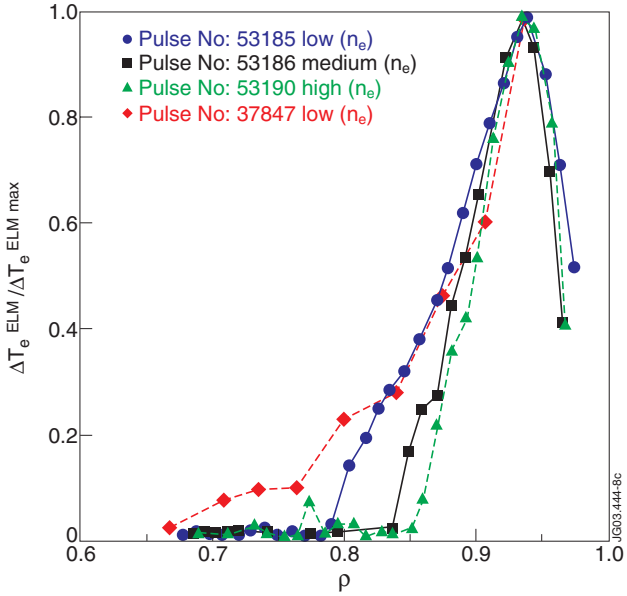

Figure 8: (b) Normalised ELM temperature perturbation ($\Delta T_e^{ELM}/\Delta T_e^{ELM\text{-}max}$) versus normalised radius (ρ = r/a) for the same series of discharges in JET and JT-60U as Fig.8(a) showing the small change of ELM affected volume with increasing plasma density.

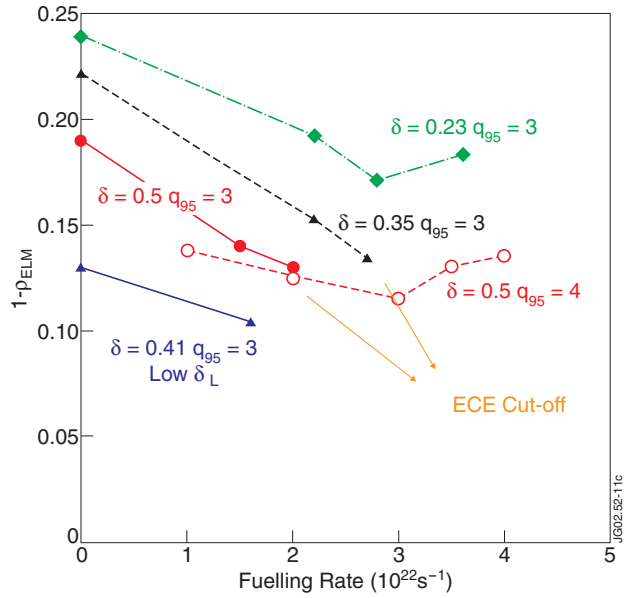

Figure 9: Normalised radial extent (ρ = r/a) of the ELM affected zone for JET discharges in various magnetic configurations versus fuelling rate. The radial extent of the ELM affected zone depends mainly on the magnetic configuration, being only weakly dependent on the rate of gas fuelling for every configuration. Discharges with higher fuelling rates and Type I ELMs exist for (δ =0.35 q_{95} =3 and δ = 0.5 and q_{95} =3), but the pedestal density is larger than the cut-off density for the ECE second harmonic emission, which is used in these measurements of the ELM affected zone. This is indicated by the ECE cut-off label in the figure.

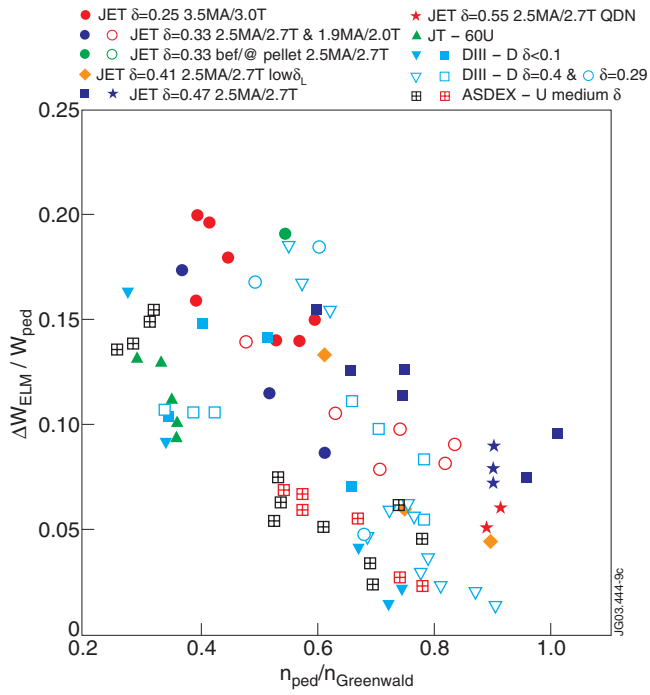

Figure 10: Normalised ELM energy loss ($\Delta W_{ELM}/W_{ped}$) versus pedestal density (normalised to the Greenwald limit) for a large range of Type I ELMy H-mode plasmas in ASDEX Upgrade, DIII-D, JT-60U and JET including various plasma triangularities, ratios of $P_{INPUT}/P_{L\text{-}H}$ and pellet triggered ELMs.

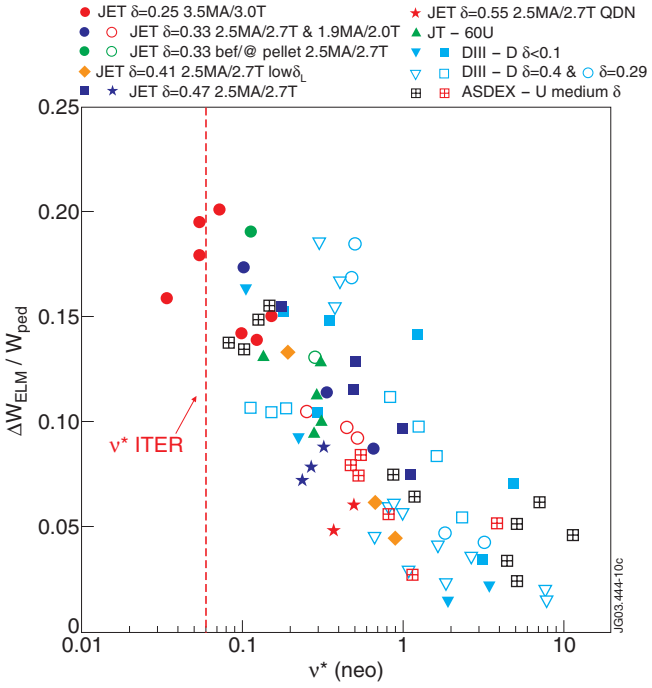

Figure 11: Normalised ELM energy loss ($\Delta W_{ELM}/W_{ped}$) versus pedestal plasma collisionality for a large range of Type I ELMy H-mode plasmas in ASDEX Upgrade, DIII-D, JT-60U and JET including various plasma triangularities, ratios of P_{INPUT}/P_{L-H} and pellet triggered ELMs.

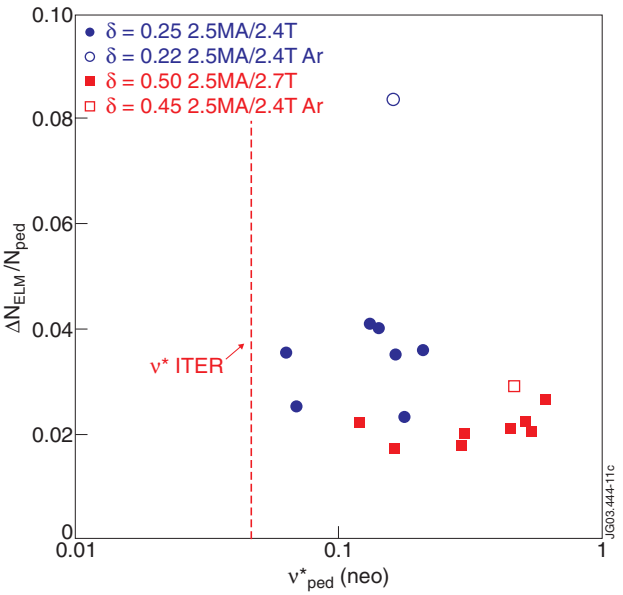

Figure 12: Normalised ELM particle loss ($\Delta N_{ELM}/N_{ped}$) versus pedestal plasma collisionality for a range of Type I ELMy H-mode plasmas in JET.

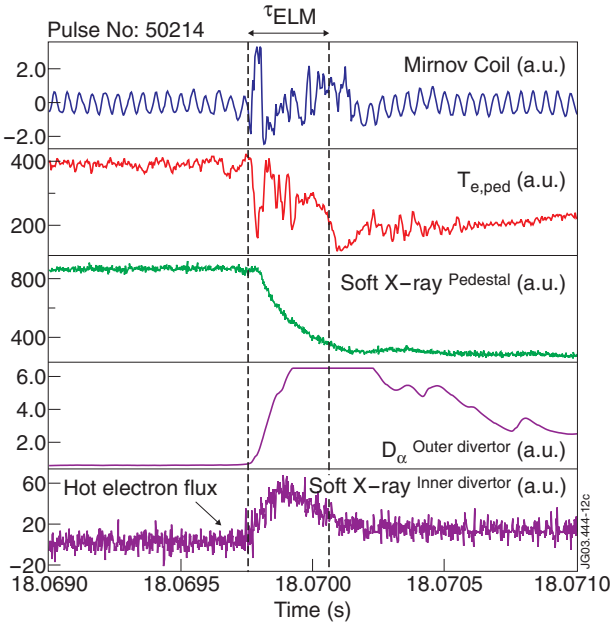

Figure 13: Measurements with high time resolution (~4 μs) of the MHD activity (measured with Mirnov coils), pedestal temperature ($T_{e,ped}$) and soft X-ray emission collapse, and outer divertor D_α emission and inner divertor X-ray bremsstrahlung from hot electron impact during a Type I ELM in JET. The collapse of $T_{e,ped}$, pedestal soft X-ray emission and inner divertor bremsstrahlung emission occur over a time interval of 200–300μs similar to the period of large MHD activity.

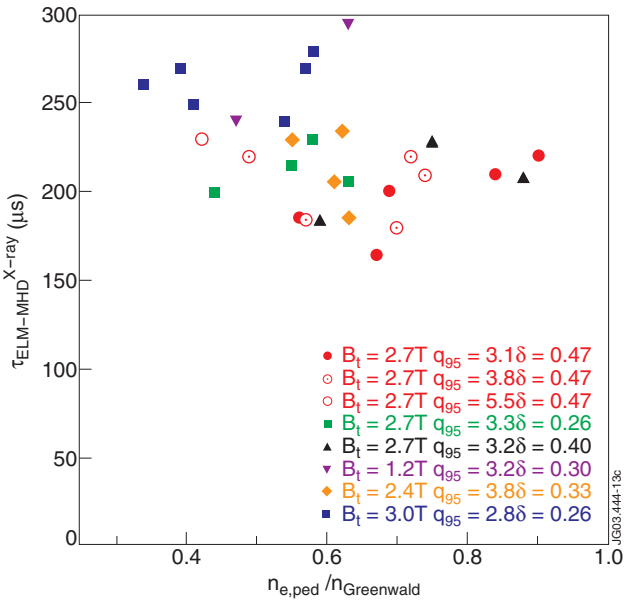

Figure 14: Time duration of the edge plasma collapse measured by the edge soft X-ray emission for a large range of JET Type I ELMy H-mode plasmas.

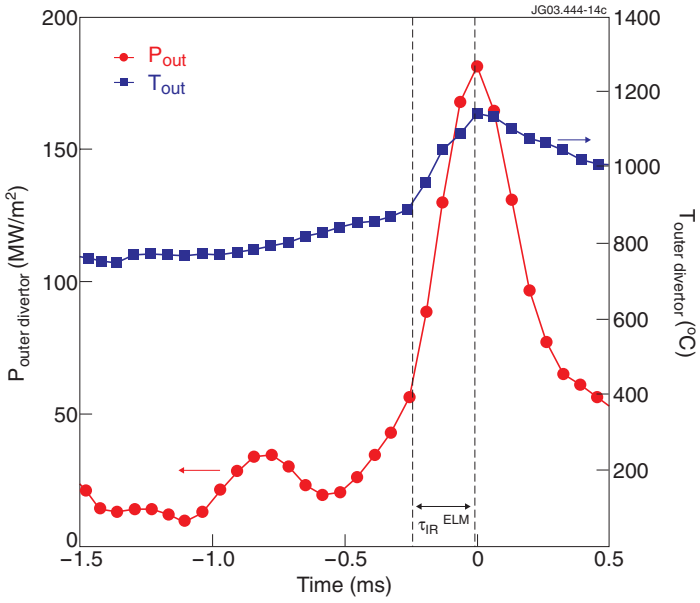

Figure 15: Time evolution of the surface temperature of the outer divertor target and the deduced power flux, for typical low/medium density ELMy H-mode conditions in JET. For inter-machine comparisons, the duration of the ELM power is characterised by the rise time of the surface temperature during the ELM (τ_{IR}^{ELM}), as illustrated in this figure.

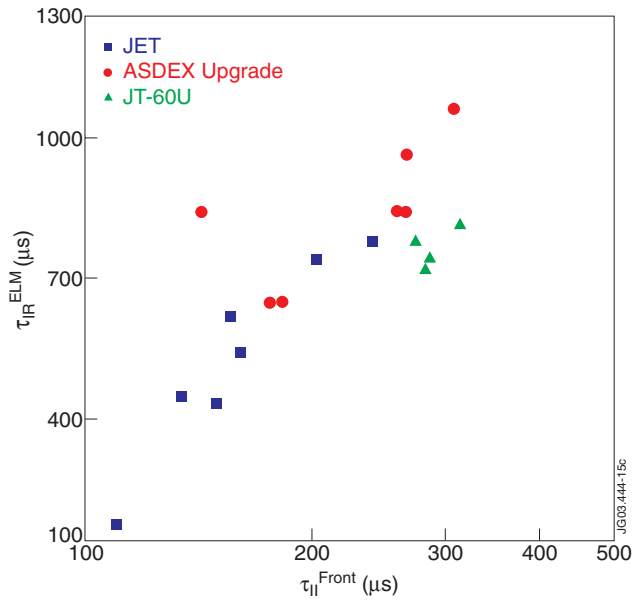

Figure 16: Duration of the ELM power pulse from infrared measurements for Type I ELMs (τ^{ELM}_{IR}) in ASDEX Upgrade, JET and JT-60U versus the SOL ion flow parallel time calculated for the pedestal plasma parameters ($\tau_{||}^{Front}$). $\tau_{||}^{Front}$ increases with decreasing pedestal plasma temperature.

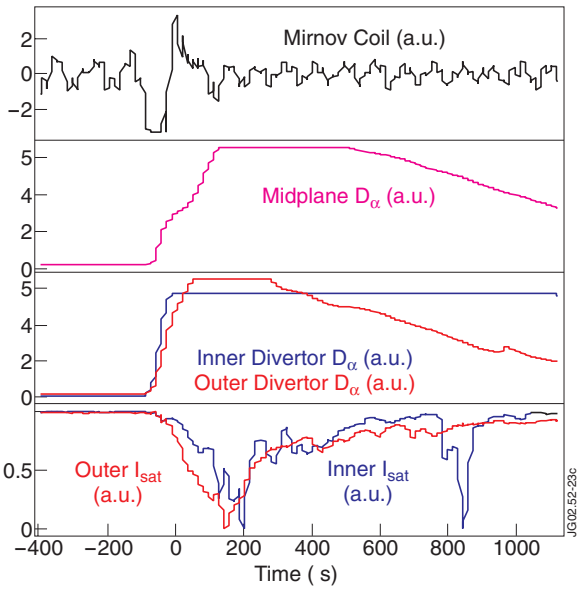

Figure 17: (a) Measurements with high time resolution (~4μs) of the ELM particle fluxes to first wall components at various locations (inner and outer divertor) in JET, as measured by the D_α emission and Langmuir probe measurements near both separatrix strike points. This ELM occurs at low pedestal densities ($n_{e,ped}$ = 5.2×10^{19}m^{-3}, $T_{e,ped}$= 1650 eV) and the increase of particle fluxes at both divertors is approximately simultaneous.

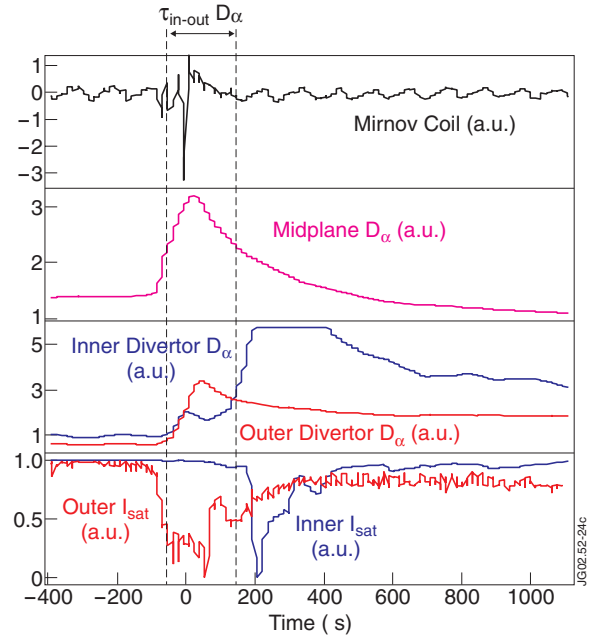

Figure 17: (b) Measurements with high time resolution (~4μs) of the ELM particle fluxes to first wall components at various locations (inner and outer divertor) in JET, as measured by the D_α emission and Langmuir probe measurements near both separatrix strike points. This ELM occurs at medium pedestal densities ($n_{e,ped}$ = 6.4× 10^{19}m^{-3}, $T_{e,ped}$= 850 eV) and the increase of the particle flux at the inner divertor is delayed with respect to that at the midplane and outer divertor by ~ 200 – 300μs.

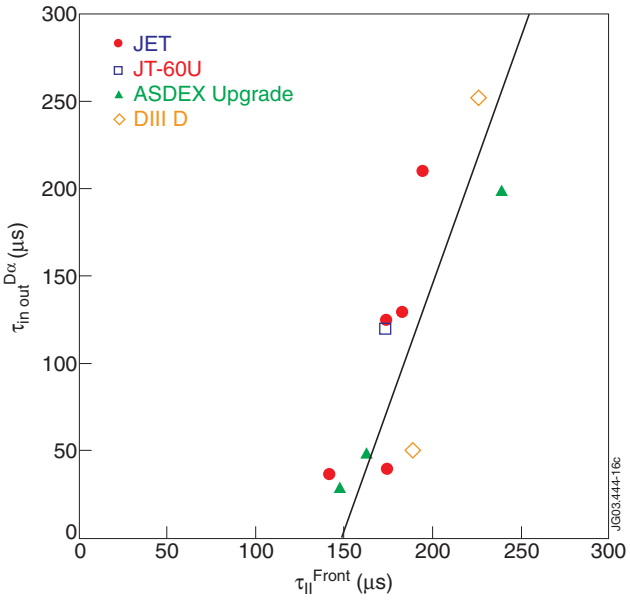

Figure 18. Measured delay between the D_α emission rise time at the inner divertor with respect to the outer divertor versus SOL ion flow parallel time calculated for the pedestal plasma parameters ($\tau_{||}^{Front}$), for a range of Type I ELMy H-mode plasmas in ASDEX Upgrade, DIII-D, JT-60U and JET.

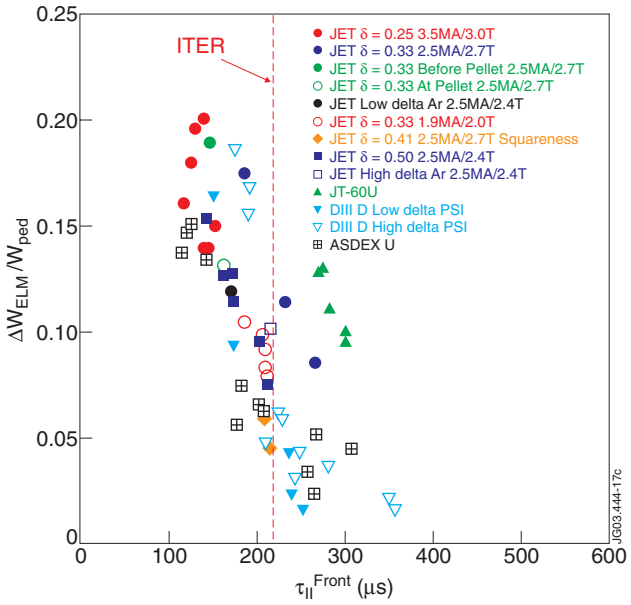

Figure 19. Normalised ELM energy loss ($\Delta W_{ELM}/W_{ped}$) versus SOL ion flow parallel time calculated for the pedestal plasma parameters ($\tau_{||}^{Front}$), for a large range of Type I ELMy H-mode plasmas in ASDEX Upgrade, DIII-D, JT-60U and JET including various plasma triangularities, ratios of P_{INPUT}/P_{L-H}, impurity seeding (Ar) and pellet triggered ELMs.

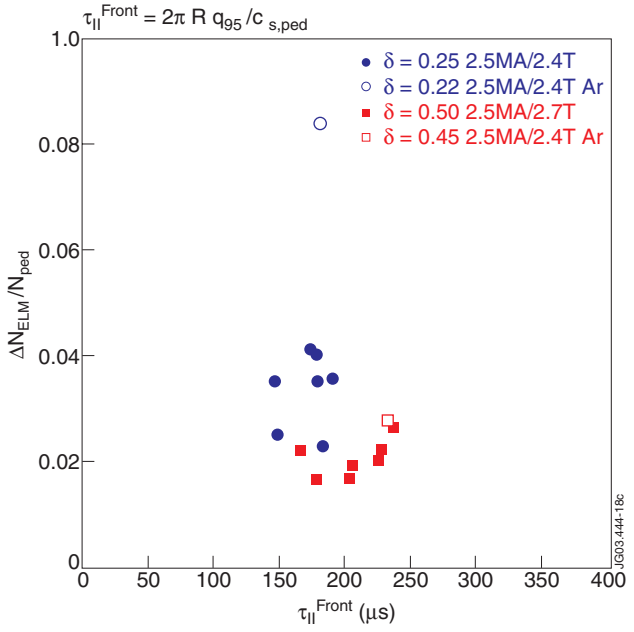

Figure 20. Normalised ELM particle loss ($\Delta N_{ELM}/N_{ped}$) versus SOL ion flow parallel time calculated for the pedestal plasma parameters ($\tau_{||}^{Front}$), for a range of Type I ELMy H-mode plasmas in JET.